Journal of Biomedical Optics

BiomedicalOptics.SPIEDigitalLibrary.org

Coregistered autofluorescence-optical coherence tomography imaging of human lung sections

Hamid Pahlevaninezhad
Anthony M. D. Lee
Stephen Lam
Calum MacAulay
Pierre M. Lane

SPIE.

Coregistered autofluorescence-optical coherence tomography imaging of human lung sections

Hamid Pahlevaninezhad,* Anthony M. D. Lee, Stephen Lam, Calum MacAulay, and Pierre M. Lane
BC Cancer Research Center, 675 West 10th Avenue, Vancouver, British Columbia V5Z 1L3, Canada

Abstract. Autofluorescence (AF) imaging can provide valuable information about the structural and metabolic state of tissue that can be useful for elucidating physiological and pathological processes. Optical coherence tomography (OCT) provides high resolution detailed information about tissue morphology. We present coregistered AF-OCT imaging of human lung sections. Adjacent hematoxylin and eosin stained histological sections are used to identify tissue structures observed in the OCT images. Segmentation of these structures in the OCT images allowed determination of relative AF intensities of human lung components. Since the AF imaging was performed on tissue sections perpendicular to the airway axis, the results show the AF signal originating from the airway wall components free from the effects of scattering and absorption by overlying layers as is the case during endoscopic imaging. Cartilage and dense connective tissue (DCT) are found to be the dominant fluorescing components with the average cartilage AF intensity about four times greater than that of DCT. The epithelium, lamina propria, and loose connective tissue near basement membrane generate an order of magnitude smaller AF signal than the cartilage fluorescence.
[DOI: 10.1117/1.JBO.19.3.036022]

Keywords: autofluorescence imaging; optical coherence tomography; human lung components; histology; cartilage; connective tissue.

Paper 130796RR received Nov. 6, 2013; revised manuscript received Feb. 7, 2014; accepted for publication Mar. 3, 2014; published online Mar. 31, 2014.

1 Introduction

Autofluorescence (AF) is the emission of light by endogenous fluorophores in biological structures when illuminated with excitation light. In tissue, the most diagnostically useful fluorophores excited by blue excitation light are collagen, elastin, and nicotinamide adenine dinucleotide phosphate.[1] The intensity and spectrum of tissue AF are determined by the quantity of fluorophores *in situ* as well as their biochemical environment. Thus changes in the intensity and spectral distribution of tissue AF can be used to follow pathological processes such as carcinogenesis.

For lung cancer, techniques for the detection of neoplastic lesions in the intraepithelial (preinvasive) stage are extremely important as their treatment leads to better patient outcomes.[2] Compared to conventional white light bronchoscopy, AF bronchoscopy has proven to be more sensitive (up to six times) in the detection of intraepithelial neoplastic lesions.[3–6] Normal tissue emits pale-green tissue fluorescence when illuminated with blue light (410 to 460 nm) primarily due to elastin and collagen content in the submucosa. The increased number of cells with larger nuclear to cytoplasmic ratios, more active metabolic state, destruction of extracellular matrix, and increased blood content associated with abnormal tissue results in the emission of markedly dimmer green AF with increased relative red AF emissions.

Human bronchi consist of different tissue components including epithelium, lamina propria, smooth muscle, hyaline cartilage, connective tissue, glands, and blood vessels. The AF intensity from each component is a measure of fluorophore content *in situ*. The information about relative AF signal intensities originating from lung tissue components is important as it can be used to model the components in terms of their biochemical properties. For instance, the spatial density of highly fluorescing collagen and elastin fibers can be estimated in the lung by endoscopic AF imaging. However, AF intensity at the surface of the tissue includes the absorption and scattering of light by different tissue layers. Optical scattering and absorption of excitation and emission light as it passes through the epithelium and stroma can significantly affect the observed tissue AF.[7] Therefore, the AF signal associated with different components cannot be accurately determined by measuring the AF intensity at the tissue surface alone as the AF intensity is altered by the scattering and absorption of intervening layers.

Optical coherence tomography (OCT) is an interferometric technique for obtaining subsurface tissue morphology, providing images with <10-μm axial resolution and >1-mm penetration depth.[8–10] When used in combination AF-OCT imaging systems can provide biochemical information colocalized with structural information. Combined OCT and AF imaging has been reported previously using different implementations. One approach was to have the two separate imaging systems combined together either in free space using dichroic mirrors[11–16] or by using an endoscopic probe with separate adjacent fibers for the two modalities.[17–23] Double-clad fiber-based endoscopic dual-modality systems have been reported with common paths for the two modalities.[24–31] Another reported approach used a single Ti-Sapphire broadband femtosecond (fs) laser source for both spectral domain OCT and multiphoton excited

*Address all correspondence to: Hamid Pahlevaninezhad, E-mail: hpahleva@bccrc.ca

fluorescence imaging.[32–39] There also have been studies on the applications of dual-modality AF-OCT imaging systems for imaging aorta samples,[11] a human breast cancer xenograft model,[15] mouse alveolar[16] and colon[20–23] tissue, *ex vivo* rabbit arteries[27] and esophagus,[28] excised sheep lung,[31,40] a rat ovarian carcinogenesis model,[41] rat bladder,[19,42] fish cornea,[32] and diseased cadaver human coronary arteries.[14,43] However, to our knowledge, there have been no published studies on AF-OCT imaging of *ex vivo* human lung sections.

In this work, we present experimental results from coregistered AF-OCT imaging of sectioned *ex vivo* human lung samples. The airway sections cut perpendicular to the airway axis in order to expose the airway wall components and to measure the AF signal intensity originating directly from these components, excluding scattering and absorption loss introduced by the other layers. We use OCT coregistered with AF imaging along with the histological evaluation to identify airway components of the *ex vivo* human lung sections. Combining the two modalities was achieved in free space using a dichroic mirror as this method offered a simple, practical approach suitable for imaging *ex vivo* sections.

2 Materials and Methods

2.1 *Tissue Preparation*

Two fresh human airways approximately 8 mm in length and 8 mm in diameter were disected from a surgically resected lung lobe removed for cancer treatment. The airways were taken from normal peritumor locations. The fresh specimens were immediately mounted and frozen in a minimal amount of optimal cutting temperature (O.C.T.) compound (TissueTek, Torrance, California) on a cryostat block holder with the airway axis perpendicular to the cutting blade. For the first specimen, a 600-μm thick section for AF-OCT imaging and an adjacent 5-μm thick section for histology were cut and placed on glass slides and allowed to thaw. A 200-μm thick section and a 400-μm thick section for AF-OCT imaging and a 5-μm thick section for histology were cut perpendicular to the luminal axis from the second specimen. The 5-μm thick sections were hematoxylin and eosin stained, mounted, and scanned on a slide scanner (Panoramic MIDI Scanner, 3DHisttech, Budapest, Hungary).

2.2 *AF-OCT Imaging System*

Coregistered AF–OCT images were acquired using a custom benchtop dual-modality imaging system. The OCT subsystem included a 30 mW polygon-scanner-based wavelength-swept laser source, built based on the system described in Ref. 44, with 106.8-nm bandwidth centered at 1321.4 nm with 40-kHz repetition frequency. This laser source fed a fiber-based Mach-Zehnder interferometer (MZI) with reference and sample arms, as shown in Fig. 1 (OCT inset). Another MZI unit was used at the source to generate the reference clock for sampling. The interference was detected by a balanced photodetector (PDB420A, ThorLabs, Newton, New Jersey) whose output was fed into a digitizer card (ATS460, AlazarTech, Pointe-Claire, Quebec, Canada) for signal processing and OCT image display. Given the OCT source bandwidth and center wavelength, the OCT subsystem axial resolution was expected to be about 8 μm. However, experimental measurements of the axial resolution by imaging through a cover slip resulted in an axial point spread function with about 11 μm full width at half-maximum. This discrepancy between the expected and measured axial resolutions could be attributed to the nonuniform spectral response of the optical components between the source and the detector. The lateral resolution was also measured to be 20 μm using the knife-edge technique.

The AF imaging subsystem used a 446 nm, 40 mW semiconductor laser (CUBE 445-40C, Coherent, Santa Clara, California) as the excitation source. An objective lens (NA = 0.3) with 40 mm working distance collected the AF signal from the sample and another lens was used to focus the collected signal onto an avalanche photodiode-based detector (C5460, Hamamatsu, Japan). A dichroic beamsplitter separated backscattered blue light from AF photons as shown in Fig. 1 (AF inset). The OCT and AF light beams were combined and separated by a backside-polished broadband dielectric mirror (BB1-E02P, ThorLabs, Newton, New Jersey) in free space. A galvo-scanning mirror (GVS002, ThorLabs, Newton, New Jersey) provided a two-dimensional (2-D) raster scan of both the AF and OCT beams on the sample. The AF and OCT channels were recorded simultaneously on the same high speed digitizer ensuring their coregistration.

2.3 *Segmentation*

Although histology is the gold standard for the study of tissue morphology, the shape and the size of the tissue components do not necessarily remain intact during the fixation, embedding, and sectioning processes. Although OCT cannot provide tissue morphology as detailed as can histology, it is possible to identify bulk tissue components in the OCT images, using an adjacent histology sections as a guide and then refer to the coregistered AF images to quantify the AF of the identified tissue components. Therefore, we used OCT en-face sections (C-scans) in combination with the adjacent histology sections to identify tissue components. The volumetric OCT images of the samples with $624 \times 720 \times 170$ pixels were acquired by a 2-D raster scan of the OCT beam on a 6×7 mm^2 area on the samples with the

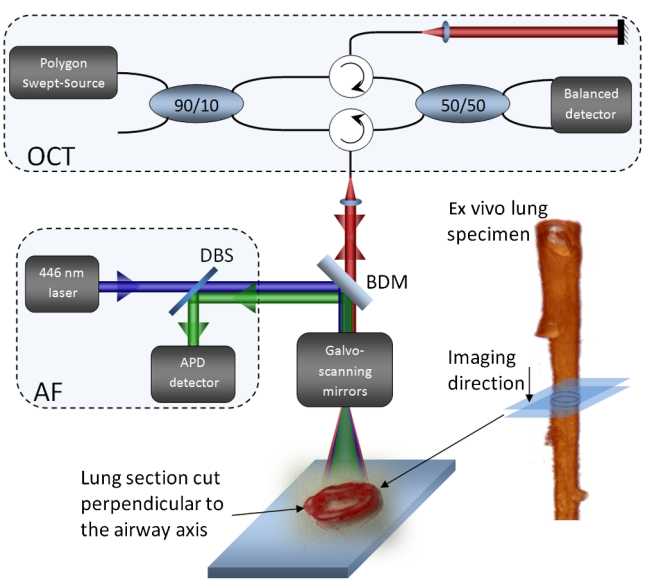

Fig. 1 Autofluorescence and optical coherence tomography (AF-OCT) imaging system, dichroic beamsplitter (DBS), and backside-polished dielectric mirror (BDM).

1-mm depth information. The three-dimensional (3-D) image was constructed from individual OCT frames and sectioned into the en-face planes perpendicular to the excitation light. The en-face OCT sections were used to segment tissue components. Cartilage areas (CAR) were found to be the most distinct areas in the en-face OCT sections as they were relatively brighter compared to the neighboring tissue. We used the en-face OCT sections in which the CAR were the most distinguishable and manually segmented CAR with ImageJ. Since dense connective tissues (DCTs) include more densely packed particles compared to loose connective tissues, they show higher scattering. Therefore, in the en-face OCT sections, DCT areas can be identified as the brighter regions compared to the neighboring loose connective tissues. We manually segmented these brighter regions as DCTs using ImageJ in the en-face OCT sections. Given the histology image, the darker regions in the en-face OCT sections near lumen included loose connective tissue, basement membrane, and epithelium. These areas were also segmented in the en-face OCT sections. The AF intensities corresponding to each component in the OCT images were quantified from the coregistered AF images. The mean value and standard deviation of AF signal over each tissue segment were obtained as the quantitative measures of AF signal for that segment.

3 Results and Discussion

Figure 2(c), the histology image of the 5-μm thick section from the first specimen, illustrates the CAR, DCTs, and other lung components, such as epithelium (Epi) and loose connective tissue. Figure 2(a) shows an en-face OCT section close to the bottom of the 600-μm thick sample. As explained previously, the 3-D OCT image was constructed from individual OCT frames (Video 1: OCT B-scans of the 600-μm thick sample (MOV, 14782 KB), URI: http://dx.doi.org/10.1117/1.JBO.19.3.036022.1) and the en-face OCT images (Video 2: en-face OCT images of the 600-μm thick sample (MOV, 20370 KB), URI: http://dx.doi.org/10.1117/1.JBO.19.3.036022.2) were constructed by sectioning the 3-D OCT image perpendicular to the excitation beam. Coregistered with the AF image, these en-face OCT images are required for the identification of the lung components and thereby their corresponding AF signal. Cartilage and DCT areas along with the areas including loose connective tissue, basement membrane, and epithelium were segmented in the en-face OCT images as illustrated in Fig. 2(a). The five CAR were the distinct features in the en-face OCT images specified by the blue lines in Fig. 2(a). Given the histology image, we believe that the bright areas in the en-face OCT image specified by the black lines in Fig. 2(a) were DCTs since they had higher OCT scattering compared to the more interior loose connective tissue and, therefore, they appeared brighter in the OCT images. The darker areas closer to the center, specified by the red lines in Fig. 2(a), included loose connective tissues, the lamina propria, and the epithelium according to the histology image. The corresponding segments were transferred to the normalized AF image by ImageJ, as illustrated in Fig. 2(b). Since the AF signal of the epithelium, lamina propria, and loose connective tissue were significantly smaller than that of cartilage and DCT, the logarithmic scale was chosen for the AF image in order to reveal more details about the AF signals of different components. The highest AF intensity was generated in the cartilage. DCTs emitted a higher AF signal compared to the loose connective tissue adjacent to the epithelium. The epithelium and the lamina propria generate a small AF signal compared to the cartilage and DCTs.

Figure 2(d) compares quantitatively the AF signals of five cartilage segments (blue diamonds), seven DCT segments

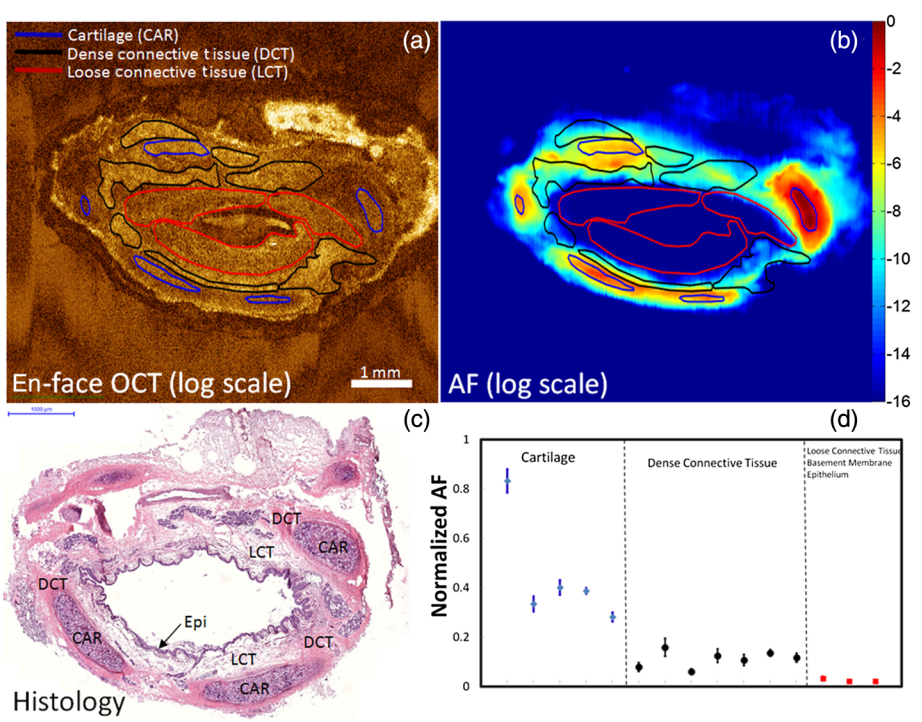

Fig. 2 (a) Segmented en-face OCT and (b) segmented AF signal in logarithmic scale of the 600-μm thick sample, (c) histology image of the adjacent 5-μm thick sample (Epi: epithelium), and (d) normalized AF for segments of the 600-μm thick sample.

(black circles), and three red segments including loose connective tissue, basement membrane, and epithelium (red squares) of the 600-μm thick sample. For each segment, the mean and standard deviation values of the AF signal were calculated over the area. The average of the AF mean values of the CAR was about four times larger than that of the DCTs and about 17 times higher than that of areas including the loose connective tissue, the basement membrane, and the epithelium. Cartilage shows significantly higher AF compared to DCT ($p = 0.0013$) and loose connective tissue, basement membrane, and epithelium ($p = 0.0001$). In addition, DCT shows significantly higher AF compared to loose connective tissue, basement membrane, and epithelium ($p = 0.0009$).

Figure 3 shows the results from AF-OCT imaging of the 200- and 400-μm thick samples. Five CAR can be identified in the en-face OCT images (Video 3: en-face OCT images of the 200-μm thick sample (MOV, 11557 KB), URI: http://dx.doi.org/10.1117/1.JBO.19.3.036022.3, and Video 4: en-face OCT images of the 400-μm thick sample (MOV, 19582 KB), URI: http://dx.doi.org/10.1117/1.JBO.19.3.036022.4). Two en-face OCT sections close to the bottom of the two samples are illustrated in Figs. 3(a) and 3(b), respectively. However, unlike the 600-μm thick sample, the only connective tissues that can be identified as bright areas in the en-face OCT images of the 200- and 400-μm thick samples were the ones surrounding the CAR. Figures 2(c) and 2(d) show the corresponding normalized AF signals. The highest AF signal was generated in the CAR. DCTs near the cartilage emitted a higher AF signal compared to the loose connective tissue adjacent to the epithelium. The epithelium and the basement membrane generated a small AF signal compared to the cartilage and DCTs. The spot size of the blue excitation light was measured to be about 20 μm. However, since the AF excitation light was scattered and not well-localized inside the tissue, the AF signal in the connective tissues surrounding the CAR might be affected by the cartilage AF emission. Therefore, we did not perform the quantitative analysis on these samples, since the connective tissues enclosing the cartilage were very close to the cartilage and their measured

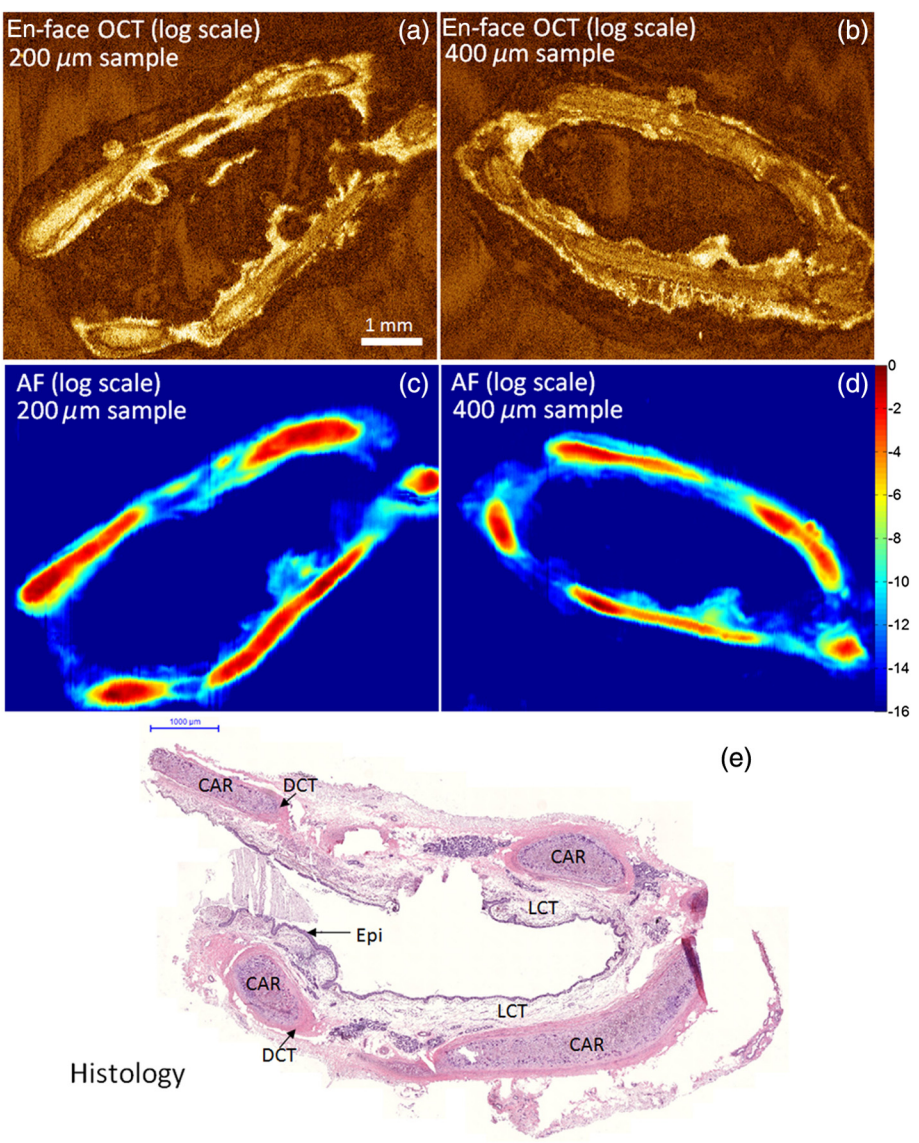

Fig. 3 OCT en-face of the 200-μm sample (a) and 400-μm sample (b), AF signal in logarithmic scale of the 200-μm sample (c), 400-μm sample (d), and the histology image of the adjacent 5-μm section of this specimen (e).

AF signals were likely to be affected by the cartilage AF signal. The histology image of the 5-μm thick section corresponding to this specimen is shown in Fig. 3(e).

High densities of elastin and collagen fibers are present in the areas that need more support. For instance, in the cartilage the high densities of collagen and elastic fibers give rise to its tensile strength, firmness, and resilience.[45] The fluorophore contents of these fibers result in the strong AF intensity of the cartilage. Elastin fibers constitute about 50% of connective tissue in human lung.[46–48] DCT contains thicker and more densely packed fluorescing collagen and elastin fibers with less ground substance, while loose connective tissue has less fibers and abundant ground substance. The higher elastin and collagen fiber contents of DCT give rise to the higher AF signal compared to the loose connective tissue AF signal. Epithelial cells covering the luminal surface of bronchi are not strongly fluorescent.

Note that for each sample, the AF signal was normalized to the maximum AF signal of each sample. The absolute AF signal maximum depends on the thickness of the sample with the highest value corresponding to the thickest sample (600-μm thick sample) since there are more fluorophores in the thicker samples.

It is noteworthy that the appearances of the lung components in the en-face OCT images are different from their appearances in the OCT *in vivo* imaging using rotating fiber optics probes. For instance, in the OCT *in vivo* imaging, the lumen and lamina propria are usually the brightest components since they are the first layers exposed to the OCT beam. Located deeper in the tissue, cartilage, and DCTs are usually darker in the OCT *in vivo* imaging due to the scattering and absorption of the OCT beam by the overlying layers closer to the tissue surface. However, in the AF-OCT imaging of *ex vivo* samples presented in this work, since the sections were cut perpendicular to the luminal axis, all the components were exposed almost in the same fashion to both the AF and OCT beams. Given the same exposure, the components with higher concentrations of scattering elements appear brighter. For instance, DCTs include more densely packed particles compared to the loose connective tissues and, therefore, they show higher scattering that, in turn, results in brighter appearances in the en-face OCT image.

Given the optical exposure method, the AF signal measured for each component is free from the scattering and absorption effects of overlying layer unlike the case in endoscopic imaging at the epithelial surface of the tissue. However, the results still include the scattering and absorption effects introduced within each component itself, hence, sections with small thicknesses were chosen to minimize these effects.

The airway specimens were frozen in O.C.T. compound to facilitate the cutting of thick sections for OCT imaging. The freezing process may have altered cellular and tissue morphology to some extent which, in turn, would have affected the absorption and scattering properties measured by OCT. In addition, the intensity of the AF signal generated, particularly cellular AF, may have been reduced by freezing.

4 Conclusion

In this work, we present experimental results from AF-OCT imaging of *ex vivo* human lung sections. The relative AF signals originating from subluminal tissue components in the airways, free from the effects of scattering and absorption usually due to superficial tissue layers, were obtained from thick sections cut perpendicular to the airway axis in order to expose the subluminal tissue components. Cartilage and DCT were found to be the dominant fluorescing components with the average cartilage AF intensity about four times greater than that of DCT. The epithelium, lamina propria, and loose connective tissue near basement membrane generate an order of magnitude smaller AF signal than the cartilage fluorescence. To our knowledge, this is the first study on the AF-OCT imaging of human lung sections to confirm quantitatively that the AF signal measured at the epithelial surface of human lung comes primarily from the cartilage and the connective tissue. The results of this study have important applications in modeling lung tissue components in terms of their biochemical properties. Given the data presented in this work, one can safely ignore the AF emissions from epithelium, lamina propria, and loose connective tissue and can model cartilage and DCT as the dominant fluorescent components with the AF emission of cartilage about four times higher than the DCT. The relative AF emission from the lung components represents the fluorophore contents of the components that, in turn, are related to the density of collagen and elastin fibers present in the tissue. These data could also be used for pathogenesis applications. For instance, using this method to follow the changes in AF signals of the different lung components due to early cancer development could provide valuable information about pathological processes involved in early cancer and could lead to a better understanding of how early cancer changes the structural and biochemical properties of the tissue components.

Acknowledgments

This work was supported by funding from the Michael Smith Foundation for Health and Research (MSFHR), Lotte & John Hecht Memorial Foundation, and Natural Science and Engineering Research Council (NSERC) Canada.

References

1. M. Monici, "Cell and tissue autofluorescence research and diagnostic applications," *Biotechnol. Annu. Rev.* **11**, 227–256 (2005).
2. S. Lam et al., "Localization of bronchial intraepithelial neoplastic lesions by fluorescence bronchoscopy," *Chest* **113**(3), 696–702 (1998).
3. S. Lam et al., "Detection and localization of early lung cancer by fluorescence bronchoscopy," *Cancer* **89**(S11), 2468–2473 (2000).
4. T. C. Kennedy, S. Lam, and F. R. Hirsch, "Review of recent advances in fluorescence bronchoscopy in early localization of central airway lung cancer," *Oncologist* **6**(3), 257–262 (2001).
5. J. Hung et al., "Autofluorescence of normal and malignant bronchial tissue," *Surg. Med.* **11**(2), 99–105 (1991).
6. B. J. Venmans et al., "Early detection of pre-invasive lesions in high risk patients: a comparison of conventional fiber optic and fluorescence bronchoscopy," *J. Bronchoscopy* **5**(4), 280–283 (1998).
7. H. Pahlevaninezhad et al., "Multimodal tissue imaging: using co-registered optical tomography data to estimate tissue autofluorescence intensity change due to scattering and absorption by neoplastic epithelial cells," *J. Biomed. Opt.* **18**(10), 106007 (2013).
8. D. Huang et al., "Optical coherence tomography," *Science* **254**(5035), 1178–1181 (1991).
9. J. G. Fujimoto et al., "Optical biopsy and imaging using optical coherence tomography," *Nat. Med.* **1**(9), 970–971 (1995).
10. G. J. Tearney et al., "In vivo endoscopic optical biopsy with optical coherence tomography," *Science* **276**(5321), 2037–2039 (1997).
11. J. K. Barton, F. Guzman, and A. Tumlinson, "Dual modality instrument for simultaneous optical coherence tomography imaging an fluorescence spectroscopy," *J. Biomed. Opt.* **9**(3), 618–623 (2004).
12. S. Yuan et al., "Three-dimensional coregistered optical coherence tomography and line-scanning fluorescence laminar optical tomography," *Opt. Lett.* **34**(11), 1615–1617 (2009).

13. S. Yuan et al., "Co-registered optical coherence tomography and fluorescence molecular imaging for simultaneous morphological and molecular imaging," *Phys. Med. Biol.* **55**(1), 191–206 (2010).
14. J. Park et al., "A dual-modality optical coherence tomography and fluorescence lifetime imaging microscopy system for simultaneous morphological and biochemical tissue characterization," *Biomed. Opt. Express* **1**(1), 186–200 (2010).
15. Y. Chen et al., "Integrated optical coherence tomography (OCT) and fluorescence laminar optical tomography (FLOT)," *IEEE J. Sel. Top. Quantum Electron.* **16**(4), 755–766 (2010).
16. M. Gaertner et al., "Investigation of alveolar tissue deformations using OCT combined with fluorescence microscopy," *Proc. SPIE* **8091**, 80911P (2011).
17. J. Y. Qu, Z. Huang, and J. Hua, "Excitation-and-collection geometry insensitive fluorescence imaging of tissue-simulating turbid media," *Appl. Opt.* **39**(19), 3344–3356 (2000).
18. R. J. McNichols et al., "Development of an endoscopic fluorescence image guided OCT probe for oral cancer detection," *Proc. SPIE* **4254**, 23 (2001).
19. Y. T. Pan et al., "Enhancing early bladder cancer detection with fluorescence-guided endoscopic optical coherence tomography," *Opt. Lett.* **28**(24), 2485–2487 (2003).
20. A. R. Tumlinson et al., "A miniature endoscope for simultaneous OCT-LIF measurement," *Appl. Opt.* **43**(1), 113–121 (2004).
21. L. P. Hariri et al., "Endoscopic optical coherence tomography and laser-induced fluorescence spectroscopy in a murine colon cancer model," *Lasers Surg. Med.* **38**(4), 305–313 (2006).
22. R. A. Wall, G. T. Bonnema, and J. K. Barton, "Novel focused OCT-LIF endoscope," *Biomed. Opt. Express* **2**(3), 421–430 (2011).
23. A. M. Winkler et al., "In vivo, dual-modality OCT/LIF imaging using a novel VEGF receptor-targeted NIR fluorescent probe in the AOM-treated mouse model," *Mol. Imaging Biol.* **13**(6), 1173–1182 (2011).
24. S. Y. Ryu et al., "Combined system of optical coherence tomography and fluorescence spectroscopy based on double-cladding fiber," *Opt. Lett.* **33**(20), 2347–2349 (2008).
25. H. Bao et al., "Nonlinear endomicroscopy using a double-clad fiber coupler," *Opt. Lett.* **35**(7), 995–997 (2010).
26. S. Lemire-Renaud et al., "Double-clad fiber coupler for endoscopy," *Opt. Express* **18**(10), 9755–9764 (2010).
27. S. Liang et al., "Intravascular atherosclerotic imaging with combined fluorescence and optical coherence tomography probe based on a double-clad fiber combiner," *J. Biomed. Opt.* **17**(7), 070501 (2012).
28. J. Mavadia et al., "An all-fiber-optic endoscopy platform for simultaneous OCT and fluorescence imaging," *Biomed. Opt. Express* **3**(11), 2851–2859 (2012).
29. D. Yelin et al., "Double-clad fiber for endoscopy," *Opt. Lett.* **29**(20), 2408–2410 (2004).
30. L. Wang et al., "Optical probe based on double-clad optical fiber for fluorescence spectroscopy," *Opt. Express* **15**(26), 17681–17689 (2007).
31. D. Lorenser et al., "Dual-modality needle probe for combined fluorescence imaging and three-dimensional optical coherence tomography," *Opt. Lett.* **38**(3), 266–268 (2013).
32. S. Tang et al., "Combined multiphoton microscopy and optical coherence tomography using a 12-fs broadband source," *J. Biomed. Opt.* **11**(2), 020502 (2006).
33. A. R. Tumlinson et al., "Endoscopic-tip interferometer for ultrahigh resolution frequency domain optical coherence tomography in mouse colon," *Opt. Express* **14**(5), 1878–1887 (2006).
34. M. T. Myaing, D. J. MacDonald, and X. Li, "Fiber-optic scanning two-photon fluorescence endoscope," *Opt. Lett.* **31**(8), 1076–1078 (2006).
35. W. Jung et al., "Design and implementation of fiber-based multiphoton endoscopy with microelectromechanical systems scanning," *J. Biomed. Opt.* **14**(3), 034005 (2009).
36. S. Tang et al., "Multiscale multimodal imaging with multiphoton microscopy and optical coherence tomography," *Opt. Lett.* **36**(24), 4800–4802 (2011).
37. G. Liu and Z. Chen, "Fiber-based combined optical coherence and multiphoton endomicroscopy," *J. Biomed. Opt.* **16**(3), 036010 (2011).
38. K. Murari et al., "Compensation-free, all-fiber-optic, two-photon endomicroscopy at 1.55 μm," *Opt. Lett.* **36**(7), 1299–1301 (2011).
39. C. Dai, X. Liu, and S. Jiao, "Simultaneous optical coherence tomography and autofluorescence microscopy with a single light source," *J. Biomed. Opt.* **17**(8), 080502 (2012).
40. J. K. Barton, A. R. Tumlinson, and U. Utzinger, "Combined endoscopic optical coherence tomography and laser induced fluorescence," Chapter 26 in *Optical Coherence Tomography, Technology and Applications*, Springer-Verlag, Berlin, Heidelberg (2008).
41. L. P. Hariri et al., "Simultaneous optical coherence tomography and laser induced fluorescence imaging in rat model of ovarian carcinogenesis," *Cancer Biol. Ther.* **10**(5), 438–447 (2010).
42. Z. G. Wang et al., "Fluorescence guided optical coherence tomography for the diagnosis of early bladder cancer in a rat model," *J. Urol.* **174**(6), 2376–2381 (2005).
43. A. M. Fard et al., "Optical coherence tomography—near infrared spectroscopy system and catheter for intravascular imaging," *Opt. Express* **21**(25), 30849–30858 (2013).
44. S. H. Yun et al., "High-speed wavelength-swept semiconductor laser with a polygon-scanner-based wavelength filter," *Opt. Lett.* **28**(20), 1981–1983 (2003).
45. V. P. Eroschenko, Chapter 3 in *Arts of Histology: With Functional Correlations*, 10th ed., pp. 55–57, Lippincott Williams & Wilkins (2005).
46. R. R. Mercer and J. D. Crapo, "Spatial distribution of collagen and elastin fibers in the lungs," *J. Appl. Physiol.* **69**(2), 756–765 (1990).
47. M. Toshima, Y. Ohtani, and O. Ohtani, "Three-dimensional architecture of elastin and collagen fiber networks in the human and rat lung," *Arch. Histol. Cytol.* **67**(1), 31–40 (2004).
48. G. Bourg-Heckly et al., "In vivo endoscopic autofluorescence microspectro-imaging of bronchi and alveoli," *Proc. SPIE* **6851**, 685104 (2008).

Biographies of the authors are not available.